INFLUENCE OF MICROSTRUCTURE ON STATIC AND CYCLIC FRACTURE TOUGHNESS OF EN-GJS-600-3 NODULAR CAST IRON

S. Hübner, P. Trubitz, S. Henschel and L. Krüger
Institute of Materials Engineering, Technische Universität Bergakademie Freiberg, Gustav-Zeuner-Straße 5, 09599 Freiberg, Germany

https://doi.org/10.1007/s40962-022-00849-y

Abstract

In this paper, the effect of microstructure of a thick-walled rotor shaft for wind turbines on fracture toughness properties has been investigated. The relevant nodular cast iron grade EN-GJS-600-3 was processed using chill casting technology. Due to different solidification conditions over the wall thickness, heterogeneous microstructures were formed. To illustrate the influence of the microstructure gradient caused by chill casting technology, specimens were taken from different sample positions in the cross section of the casting component. A detailed metallographic analysis revealed essential differences in microstructure. The crack growth resistance under quasi-static loading conditions and the fatigue crack propagation under cyclic loading conditions were measured. The results of the static fracture mechanics investigations revealed that fracture toughness is strongly influenced by the microstructure of this pearlitic ductile iron grade. On the other hand, cyclic fracture mechanics analysis showed that the complex formation of the microstructure has only a minor effect on the fatigue threshold value, but microstructure has a significant effect on the stable crack growth. For the assumed load cases, it was shown that microstructure can be a dominant factor on the mechanical and fracture toughness properties.

Keywords: *fracture mechanics, nodular cast iron, microstructure, cyclic tests, crack growth*

Introduction

In order to improve the performance of wind turbines, components made of nodular cast iron must have high strength and sufficient damage resistance, even at low temperatures. Therefore, knowledge of the mechanical and, in particular, the fracture toughness material behaviour is of great importance. For moderate stress conditions, ductile nodular cast iron EN-GJS-400-18-LT can be used for hollow rotor shafts. However, for higher stress demands, a material with sufficiently high strength, such as EN-GJS-600-3, and sufficient damage tolerance could be required. Furthermore, to combine innovative casting technology with an economical manufacturing process, chill casting technology is used in the production of high-performance hollow rotor shafts. Casting in a permanent mould with a sand core results in different solidification regimes in these thick-walled components. As a result, gradients in microstructure and material properties occur.

Recent studies[1–3] led to a comprehensive knowledge on the microstructural, mechanical and fracture toughness properties of EN-GJS-400-18-LT. For solid solution strengthened ductile cast iron components casted in permanent moulds, it was found that microstructure varied with cooling rates.[4] In particular, the number of graphite nodules was linear dependent on the solidification time. For higher-strength EN-GJS-600-3 with a structural gradient, however, the findings to date are insufficient and more investigations are necessary.

Within the framework of the design of a wind turbine, the strength of each individual component must be measured. To determine the component resistance to progressive damage and the load-bearing capacity of components, a suitable strength verification must be provided. For components subjected to cyclic loading, this assessment is performed using, among others, the fracture mechanics

Received: 04 April 2022 / Accepted: 30 June 2022 /
Published online: 8 August 2022

strength verification in accordance with the FKM guideline of the Forschungskuratorium Maschinenbau e.V.[5,6] While the assessment of fracture mechanics parameters for cyclically loaded components in wind turbines is currently being included in the certification procedure, the fracture mechanics assessment of the microstructure influence has not yet been studied in detail.

For a pearlitic nodular cast iron, Borsato et al.[7] have shown that with increasing wall thickness and solidification time there is an increasing probability for the formation of defects. A low graphite nodule count, micro-shrinkages or heterogeneous graphite nodule formation were identified. For ferritic nodular cast irons, the effect of degenerated graphite nodules as internal notches, which are a result of long solidification times, is also reported by Pusch et al.[1] Fatigue resistance clearly depends on the graphite formation. Size, shape and distribution of the graphite nodules affect crack initiation and crack propagation. Large and degenerated nodules reduce fracture toughness and cause a higher crack propagation rate.[8] Furthermore, chunky graphite was used to explain the impact of degenerated graphite nodules on the properties of ferritic nodular cast iron by Baer.[9] Degenerated graphite disrupts the matrix continuity in the loaded cross section of the material and lowers its load bearing capacity.

However, not only the characteristics of the graphite nodules depend on the solidification time, but also the formation of the metallic matrix. In a microstructure of a pearlitic matrix with Bull's-eye ferrite surrounding the graphite nodules, it is to be expected that the plastic deformation behaviour is strongly affected by the pearlitic phase on the one hand. On the other hand, the ferritic phase component ensures toughness and higher crack resistance. In Ref. 8 it was found that the ductile ferritic phase helped arresting cracks by reducing the stress intensity in front of the crack tip. The damage behaviour is therefore determined by the phase proportions which depend on the solidification time and chemical composition. So far, it has not yet been sufficiently investigated how the formation of the metallic matrix in thermal centres with longer solidification times affects the crack resistance behaviour of a pearlitic nodular cast iron.

The intention of this paper is to reveal interdependencies between the complex microstructure formation in different solidification regimes and the effects on the static and cyclic crack resistance behaviour of the nodular cast iron grade EN-GJS-600-3. Systematic tests were performed to investigate the microstructure on samples taken over the entire cross section of the thick-walled casting component and to study its effect on mechanical properties, determined in tensile tests, and fracture toughness properties. Fracture toughness values determined in the static load case as well as cyclical threshold values and parameters determined to describe stable crack growth in a cyclic load case are taken as a basis for further understanding of the microstructure influence in higher-performance casting components in the power train of wind turbines.

Materials and Methods

A hollow rotor shaft out of pearlitic nodular cast iron grade EN-GJS-600-3 (5.3201) manufactured in chill casting technology was investigated. The used casting mould system is a combination of a permanent metal mould on the outer contour and a sand core on the inside, as shown schematically in Figure 1. Due to the different heat dissipation at the mould and sand core, the solidification conditions differ throughout the casting. From the flange to the upper shaft area as well as from the outer radius of the permanent mould to the sand core in the interior, microstructural gradients over the wall thickness are to be expected due to different solidification rates, symbolized by the coloured arrows in Figure 1.

The samples were taken from different positions of the rotor shaft in order to represent the effect of microstructure on mechanical and fracture toughness properties. As sample positions, areas which are highly loaded and are relevant to damage in operating conditions due to their shaft geometry (main area, outer radius, Figure 1a) or solidification conditions (main area, inner radius and shaft head, Figure 1b) were selected. Wall thicknesses are approximately 265 mm in the main area and 330 mm in the shaft head. All samples were taken at positions that corresponded to the later outer radius after finishing. The orientation of the notch was chosen parallel to the surface of the shaft (tangential) so that the crack remains in the same microstructural area during propagation. For comparative purposes samples were also taken from a reference area with a wall thickness of approximately 218 mm (flange, Figure 1c) as hollow bore samples. From this area, samples can be also taken during regular production for quality assurance.

Analysis of the microstructure was conducted by light optical microscopy on specimens of the immediate vicinity of the crack plane of fracture mechanics specimens. Microstructural parameters were measured at unetched and etched metallographic specimens. Unetched samples were used to measure and describe the graphite morphology by mean diameter d_G and form factor f of graphite nodules and the mean distance λ between neighbouring nodules (Figure 2). Following that, the metallographic specimens were etched with a 3% nital solution and ferrite content A_F in the pearlitic matrix was determined.

Sample geometries were B6x30-specimens[10] for tensile testing (all areas, specimen form B, diameter 6 mm in the parallel length of 30 mm, M10 thread for mounting, Figure 3a), stepped notch compact tension (CT)-specimens[11]

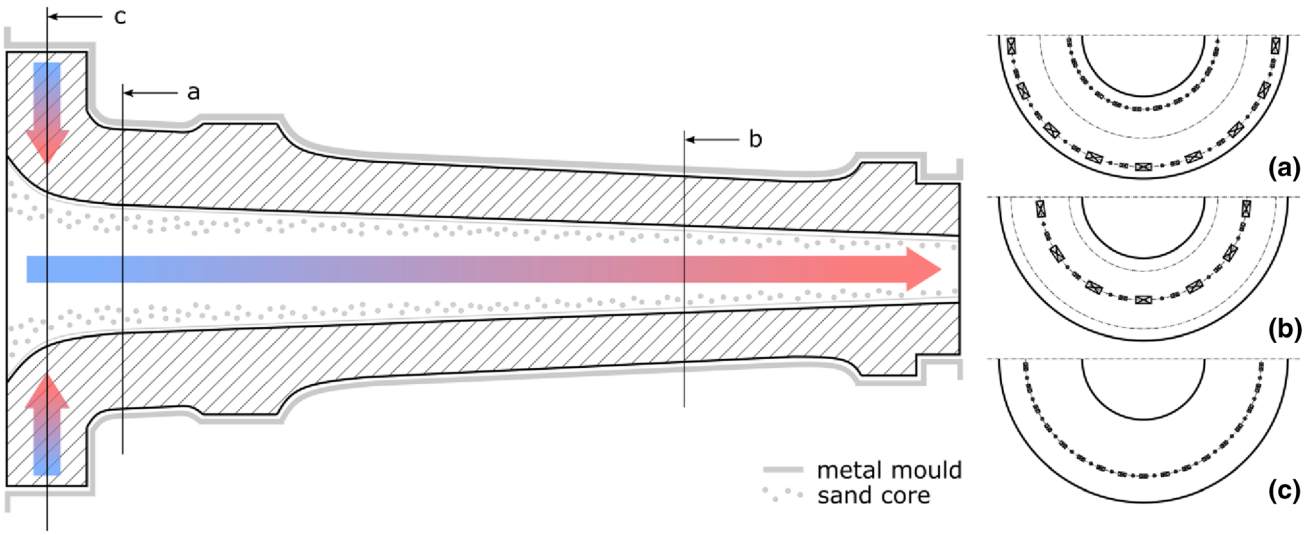

Figure 1. Sampling positions of the hollow rotor shaft: main area (a), shaft head (b) and reference area flange (c).

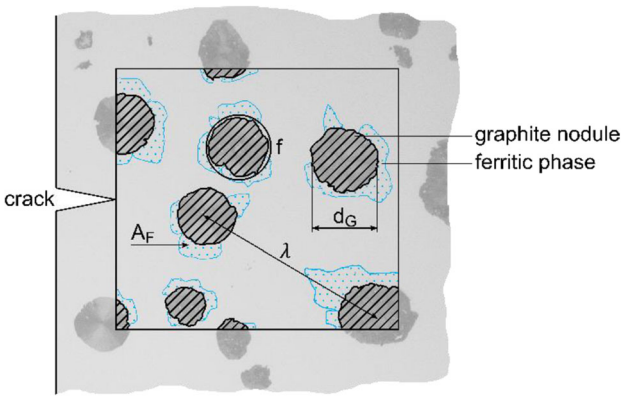

Figure 2. Determination of microstructural parameters in nodular cast iron.

for determination of static fracture toughness values (main area outside and shaft head, sample thickness 25 mm, Figure 3b) and single-edge notch bend (SENB) specimens[12] for determination of cyclic fracture toughness values (main area and shaft head, sample thickness 10 mm, Figure 3c). For gaining static fracture toughness, values from the shaft flange SENB specimens were used as well. The SENB sample geometry was used when limited material from highly loaded areas of the hollow rotor shaft was available for testing. Furthermore, reliable cyclic fracture toughness values can also be determined on this specimen geometry at $R = -1$.

Tensile properties were determined in an electromechanical universal testing machine *Zwick 1476* with attached cooling chamber at test temperatures relevant to practice. Tensile testing was conducted at room temperature and − 40 °C on specimens taken from all sample positions. The test results were compared with the required minimum values at room temperature according to Ref. 13 for EN-GJS-600-3 in the relevant wall thickness, see in Table 1. From the designation of the cast iron grade, it can be deduced that a minimum tensile strength of 600 MPa and a minimum of 3% elongation after fracture for wall thicknesses $t \leq 30$ mm is required. The wall thickness of $265 \leq t \leq 330$ mm in the component exceeds the maximum thickness specified in the standard. However, comparisons were derived on the basis of the wall thickness $60 < t \leq 200$ mm, as the required minimum values of tensile properties become smaller with increasing wall thickness. Thus, a conservative view of the tensile test results is given.

Static fracture mechanics investigations were conducted on a servo-hydraulic testing machine *MTS 880 (250 kN)*. The experiments were carried out in single-specimen procedure

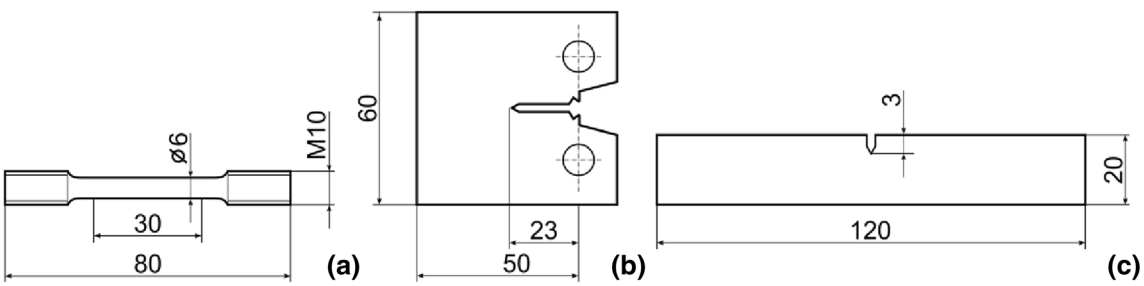

Figure 3. Test specimens B6x30 (a), CT(25) (b) and SENB (c).

Table 1. Minimum Values of Ultimate Tensile Strength, Yield Strength at 0.2% Plastic Elongation and Elongation After Fracture of EN-GJS-600-3[13]

Nodular cast iron	Matrix	Wall thickness t, in mm[13]	**UTS**, in MPa	**YS**, in MPa	***A***, in %
EN-GJS-600-3	predominantly pearlitic	$60 < t \leq 200$	550	340	1

according to the compliance method. Notch opening was measured using a clip-on gauge to determine elastic compliance of the sample which was converted into the current crack length in accordance with Ref. 11 by means of a compliance function.

In order to reveal the progress of crack propagation properly, the specimens were heat-tinted prior to crack front assessment. The evaluation of crack propagation in static fracture mechanics investigations was conducted according to ISO 12135, while crack length measurement and evaluation in the cyclic fracture mechanics tests was carried out according to ASTM E647-15e1. The evaluation of the threshold value behaviour according to ISO 12108[12] requires lower crack propagation rates than according to ASTM E647-15. Due to the microstructure, the relevant crack propagation rates may not be achieved in nodular cast iron if the crack front is stopped at graphite nodules.

The fracture mechanics investigations to determine a cyclic crack growth curve were performed on a resonance testing machine *RUMUL Mikrotron (20kN, Russenberger Prüfmaschinen AG)*. Depending on the load ratio to be achieved at the crack tip, different test setups can be used. To cover the relevant load ratios from $R = -1$ to $R = 0.5$ in the cyclic fracture mechanics test, an 8-point bending setup was used.[14] Main focus was put on the load ratio $R = -1$ as pure alternating stress is the application-relevant load case during operation of the rotor shaft in a wind turbine.

The crack propagation was evaluated by a clip-on gauge at the notch measuring the compliance at every load cycle. For conformity of crack length measurement and load control of the testing machine, an adapted compliance function and a geometry function according to Murakami[15] were used.

The threshold value ΔK_{th} was determined at R = const. under load reduction from a start value of cyclic stress intensity ΔK until the crack propagation rate had decreased to the decade relevant for evaluation according to ASTM E647-15.[16] The determination of ΔK_{th} was conducted by linear regression when sufficient pairs of measured values were available. If those requirements were not met, a nonlinear regression model was used.[17]

For each load ratio, a minimum number of 5 valid test results should be generated according to VDMA 23902.[18] One must assume that with increasing crack length and concomitant increasing crack closure, the threshold values also tend to increase as was determined in previous investigations.[19] Due to crack closure effects, these characteristic values depend on the crack length and should therefore be determined uniformly with the shortest possible crack. Therefore, tests to determine the threshold value ΔK_{th} as well as the Paris parameters m and C were conducted on separate specimens.

Results

Analysis of Microstructure Depending on Solidification Rate

Microstructure parameters determined in metallographic analyses on a large number of specimens have shown that matrix and graphite formation were strongly dependent on the sampling position and solidification times. Solidification times were modelled and were highest at the metal mould and lowest at the sand core. From the inner radius via shaft head and shaft flange to the outer radius of the rotor shaft, the content of ferritic phase A_F increased. At the same time, the values of the mean diameter of the graphite nodules d_G and the mean distance between neighbouring nodules λ decreased, while the form factor increased in the opposite direction. The sampling positions were indicated in Figure 4 as well as Table 2 by a, b, c and d. A form factor of 1 means that a graphite nodule is perfectly spherical. Therefore, decreasing form factors describe more irregular spherical shapes of the nodules. For all values concerning the graphite particles, the standard deviation increased from the outer to the inner sample position. In total, a minimum of 17.000 graphite nodules were analysed for each sampling position.

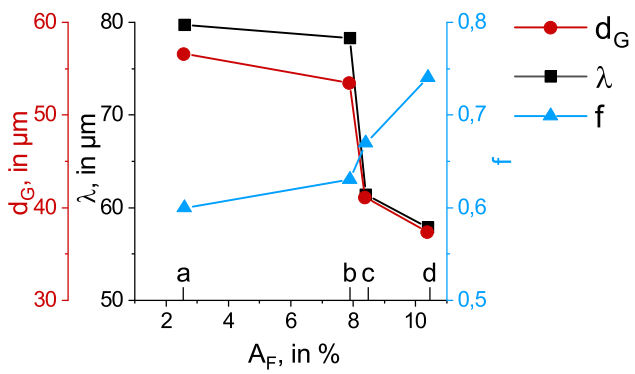

Figure 4. Microstructure parameters at the sampling positions main area, shaft head and flange.

Table 2. Solidification Times and Microstructure Parameters at the Sampling Positions Main Area, Shaft Head and Flange

Sampling position	Solidification time, in s	d_G, in μm	f	λ, in μm	A_F, in Vol.-%	Position in Figure 4
Main area (outside)	750	37.4 ± 0.9	0.74 ± 0.03	57.9 ± 2.0	10.4 ± 1.5	d
Shaft flange	2600	41.1 ± 0.5	0.67 ± 0.01	61.4 ± 0.8	8.4 ± 0.1	c
Shaft head	4750	53.5 ± 2.5	0.63 ± 0.03	78.3 ± 5.1	7.9 ± 2.1	b
Main area (inside)	4800	56.6 ± 5.1	0.60 ± 0.04	79.7 ± 7.5	2.6 ± 1.5	a

After etching, the metallographic specimens showed a pearlitic matrix with ferrite content that depended on the sampling position. In decreasing percentage from the outer to the inner radius, the ferrite was predominantly found at the grain boundaries and surrounding the graphite particles. There was a noticeably stronger formation of Bull's-eye ferrite in the outer radius and the shaft flange, even though a faster cooling rate should suppress ferrite formation. Therefore, one has to assume that pearlite stabilising alloying elements, which are added to adjust a pearlitic matrix, accumulate in the vicinity of the solidification front.

Microscopic images of the metallographic sections clearly show the dependence of microstructure parameters on the sampling position. Specimens taken from the outer radius (permanent mould, Figure 5a) and the shaft flange (both with a high solidification rate of the melt, Figure 5d) showed a fine-grained structure with small, finely distributed graphite nodules. Towards the inner radius (sand core, low solidification rate, Figure 5c), the microstructure and graphite nodules coarsened due to heat accumulation. As a diffusion controlled process, graphite particles grow to bigger nodules with longer solidification times. The carbon present in the matrix is not sufficient to serve all the nucleation sites, which means that the number of graphite nodules is low for long solidification times and their spacing is automatically greater. Due to solidification conditions in the middle layer (shaft head, Figure 5b) and inner radius as thermal hotspots, the graphite nodules showed more heterogeneity in distribution and size.

Tensile Testing

Table 3 and the stress–strain curves in Figure 6 show the results of tensile testing at room temperature and − 40 °C of specimens taken from all sample positions that were published recently.[20] It was shown that the mechanical properties of the highly loaded areas determined at room temperature mainly exceeded the minimum values required in Ref. 13 for the nodular cast iron grade and a wall thickness of $60 < t \leq 200$ mm.

Ultimate tensile strength UTS, yield strength at 0.2% plastic elongation YS and fracture elongation A showed a dependence on the sampling position. From outer to inner position of the main area, strength and ductility values decreased. While the yield strength of all sampling positions increased as expected when tested at −40 °C, the decrease in tensile strength can be explained by an embrittlement of the matrix and a decrease in plastic deformation (Table 3). It can be seen that the reference specimens from the shaft flange overestimate the strength values and underestimate the elongation values of the failure-critical main area (outside). This should be considered in future quality assurance testing.

Determination of Quasi-static Fracture Toughness

Crack resistance is determined by the microstructure and ductility of the matrix. It was expected that brittle material failure would occur due to the pearlitic matrix of EN-GJS-600-3. Indeed, the specimens of the main area (outside) and shaft head showed a wide range in damage and failure behaviour. Therefore, two scenarios had to be distinguished, depicted in Figure 7: failure of the specimen at lower loads right after the linear-elastic behaviour of the force-COD-curve (which enabled the determination of a plane strain fracture toughness value K_{Ic}, Figure 7a and failure at higher maximum loads due to elastic-plastic behaviour (determination of K_{Jc} in accordance with Ref. 21, Figure 7b. Furthermore, pronounced pop-in behaviour was detected at both testing temperatures and is exemplified in Figure 7a. A pop-in is a local discontinuity of unstable crack propagation which is stopped again by the matrix. Abrupt and significant force drops and increases of the displacement can be recorded and evaluated in accordance with Ref. 11.

The mean values of fracture toughness of the sample positions main area (outside), shaft head and flange in dependence of the testing temperature are shown in Table 4. Basically, at room temperature pronounced elastic-plastic behaviour of the samples could be observed and fracture toughness values had to be determined using the J-integral method. At the testing temperature − 40 °C, the force-COD-curve showed a mostly linear-elastic slope, followed by unstable crack extension and unstable failure. Hence, the evaluation was performed according to plane-strain fracture toughness. For the main area (outside) and shaft flange, some results again had to be evaluated in terms of J-integral method.

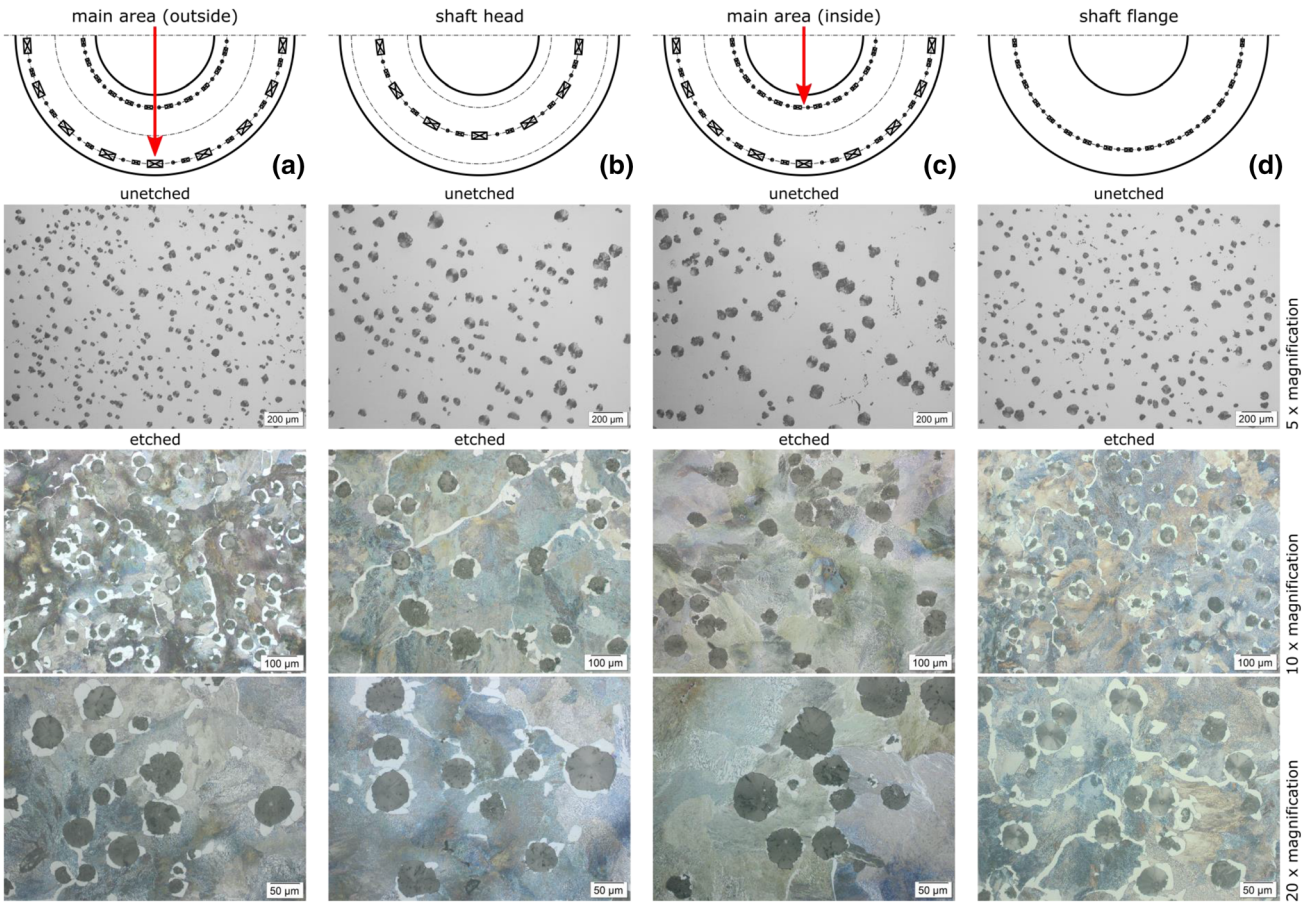

Figure 5. Microstructure at the sampling positions main area (outside, a), shaft head (b), main area (inside, c) and shaft flange (d).

Table 3. Mean Values of Ultimate Tensile Strength, Yield Strength at 0.2% Plastic Elongation and Elongation After Fracture of Specimens of All Structural Areas of the Rotor Shaft[20]

Sample position	***T***, in °C	**UTS**, in MPa	**YS**, in MPa	***A***, in %
Main area (outside)	RT	672 ± 23	408 ± 4	6.6 ± 0.9
	− 40	662 ± 18	435 ± 4	4.4 ± 1.0
Shaft head	RT	607 ± 26	404 ± 3	3.3 ± 1.4
	− 40	537 ± 38	437 ± 5	1.4 ± 0.8
Main area (inside)	RT	531 ± 11	391 ± 2	3.0 ± 1.0
	− 40	509 ± 19	422 ± 3	3.8 ± 2.9
Shaft flange	RT	679 ± 26	427 ± 5	4.5 ± 0.8
	− 40	630 ± 38	457 ± 5	2.0 ± 0.0

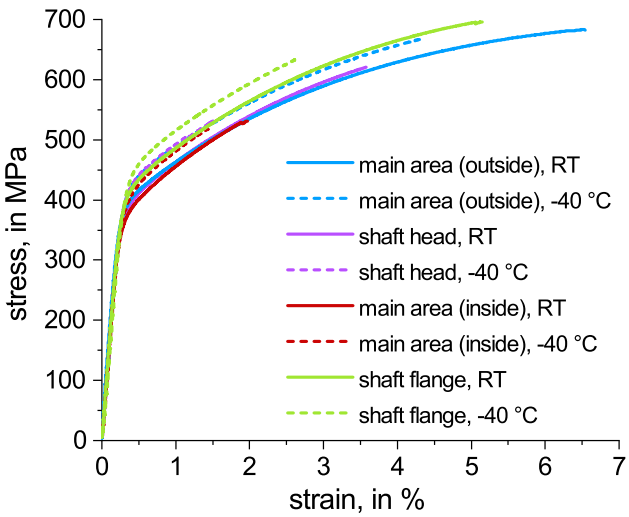

Figure 6. Stress–strain curves of all sampling positions at testing temperatures RT and − 40 °C

Considering the basics of the present work, the focus must be put on the predominantly pearlitic matrix with a finer-grained structure and a higher proportion of Bull's-eye ferrite in the outer layer of the main area. Failure behaviour is not determined exclusively by the testing temperature, but also by microstructural parameters.

For ferritic nodular cast iron and quasi-static loading conditions, from Refs. 3,22,23 it is known that at room temperature and ductile crack propagation, a higher crack resistance occurs with increasing mean diameter, increasing distance of the graphite nodules and a coarser matrix.

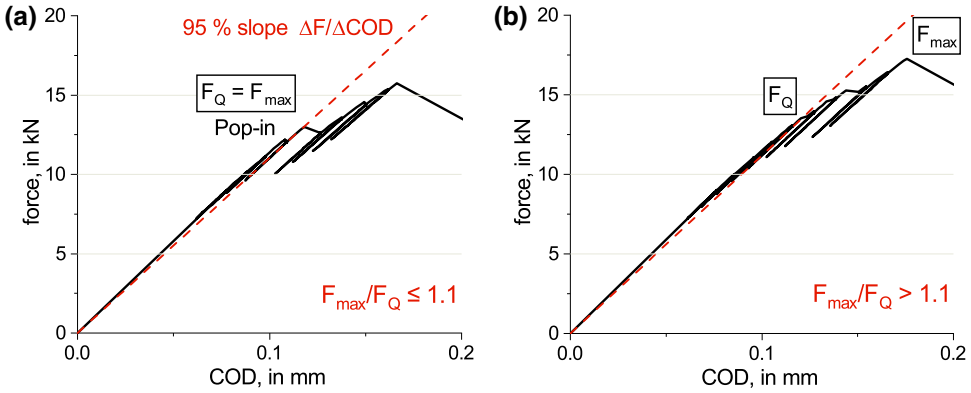

Figure 7. Exemplary F-COD-curves of the sampling position main area (outside) for determination of K_{Ic} (a) and K_{Jc} (b).

Table 4. Fracture Toughness Values of the Sampling Positions Main Area (Outside), Shaft Head and Flange as a Function of the Testing Temperature

	T, in °C	***K***, in MPa$\sqrt{m}$	Classification
Main area (outside)	20	42.8 ± 3.7	$K_{Jc(25)}$
	− 40	29.9 ± 1.4	$K_{Jc(25)}$
		24.3 ± 1.0	K_{Ic}
Shaft head	20	38.2 ± 3.1	$K_{Jc(25)}$
	− 40	21.6 ± 1.8	K_{Ic}
Shaft flange	− 40	25.2 ± 3.3	$K_{Jc(10)}$
		23.1 ± 1.1	K_{Ic}

On the other hand, small graphite nodules and a finer-grained matrix resulted in higher crack resistance for brittle material behaviour of ferritic nodular cast iron.

The present results of the examined microstructure effect showed that also the EN-GJS-600-3 with finer-grained microstructure with smaller, homogeneously distributed graphite nodules with smaller distances and larger form factors cause an increased fracture toughness at lower temperatures. Regarding the works of Baer[23] the present findings clearly help to understand that the deformation behaviour of pearlitic nodular cast iron is significantly dependent on the microstructure and testing conditions. Quasi-static crack resistance decreased with a coarser matrix and partly degenerated graphite nodules and fracture behaviour changed from ductile to brittle with decreasing testing temperature and an increasing content of pearlitic phase. If all of these findings are summarized, it can be concluded that fracture toughness values obtained at room temperature (K_{Jc}) as well as from testing at a temperature of − 40 °C (K_{Ic}) were approximately 12% higher on samples taken from the outer layer of the main area compared to the shaft head.

Thus, a clear dependence of fracture toughness on the sampling position in cross section between a permanent mould and a sand core is recognizable. The comparison of microstructural parameters of the main area (outside) and shaft flange revealed a slightly coarser microstructure with decreased content of ferritic phase in the reference position. Therefore, the decrease in fracture toughness in the shaft flange was to be expected. Again, if in future quality assurance the results are to be used to make a prediction about the properties of the main area (outside), it must be noted that in the case of quasi-static loading, the fracture toughness of the highly loaded main area is underestimated. Fracture toughness values of the flange were 5% lower than in the main area. It is therefore a conservative approach.

When evaluating the effect of the pearlitic matrix, the characteristics of the ferritic phase surrounding the graphite nodules must also be taken into account. As can be seen in the scanning electron microscope images of fracture surfaces of specimens of the main area (outside) in Figure 8, Bull's-eye ferrite caused ductile fracture zones. It is assumed that ductile fractions of the microstructure affect the damage behaviour. Therefore, the material behaviour is no longer purely linear-elastic, as was depicted in the F-COD-curve in Figure 7a. A slightly larger proportion of Bull's-eye ferrite in the outer layer seems to affect the deformation capacity in front of the crack tip in such a way that an overall elastic-plastic behaviour of the material is maintained even at low temperatures (Figure 7b). This coincides with the findings of Ref. 22 who found that there is a nonlinear relationship between fracture toughness and ferrite content for pearlitic-ferritic nodular cast irons with different phase fractions. This leads to an increased fracture toughness and, in some cases, their determination in terms of the J-integral method. Local microstructural heterogeneities and various damage processes at the crack tip lead to different requirements in determination of fracture toughness values and the material parameters obtained, therefore, are not directly comparable with each other, as shown in Figure 7.

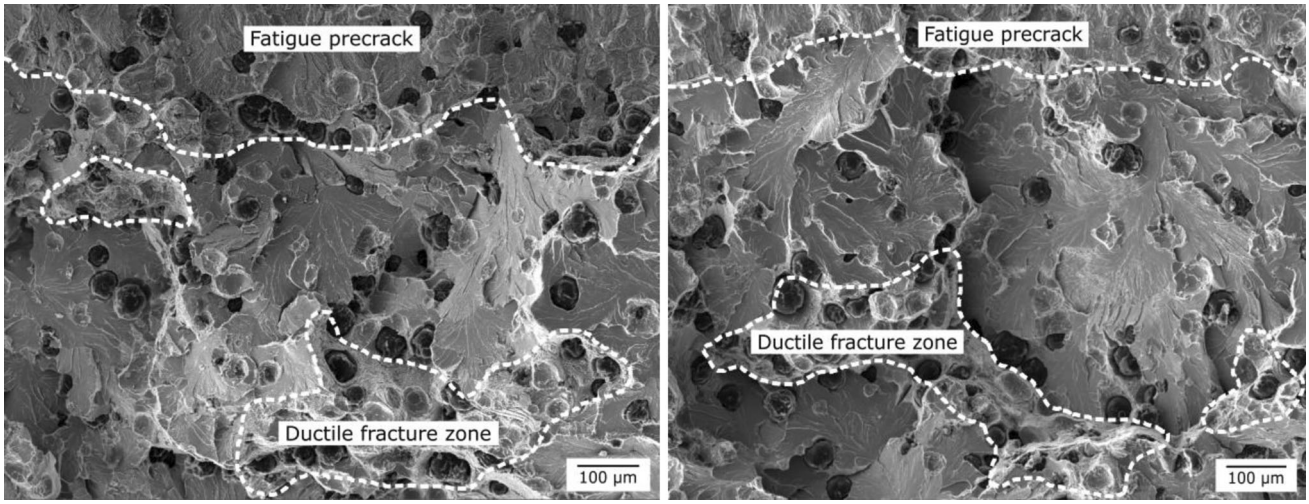

Figure 8. Scanning electron microscope images of fracture surfaces of specimens of the main area (outside): fatigue crack front (top) and ductile fracture zones (bottom, circled).

In Figure 8, the fatigue crack front and ductile fracture zones were indicated on the fracture surface image of CT(25)-samples after quasi-static loading. It can be seen that areas of more ductile microstructure are deformed more strongly and the graphite nodules are embedded in dimple-shaped ferritic phase. The surrounding brittle, pearlitic matrix can no longer relieve the local stress concentrations at defects. The local deformability is exceeded and brittle fracture occurs. It should be noted that the ductile ferritic areas surrounding the graphite nodules are not sufficient to stop unstable crack propagation (e.g. during pop-ins).

Cyclic Crack Propagation Tests

The threshold values determined at all load ratios on SENB specimens of the main area (outside) of the rotor shaft are presented in Figure 9. Table 5 shows the mean values of threshold ΔK_{th} of all failure-critical sample positions as a function of the load ratio R.

The data show that the threshold values decrease with increasing load ratio, which indicates a decreasing resistance of the nodular cast iron to crack propagation. The effect of a microstructural gradient on the threshold determination in cyclic fracture mechanics examinations is relatively low. It can be concluded that sample position and ferrite content have only a minor effect on crack initiation. This coincides with the findings of Motz et al.[24] For the reference position shaft flange, ΔK_{th} was only measured at $R = -1$. It was observed that ΔK_{th} was approximately equal to threshold values of the shaft head where a significantly coarser structure can be found. From the findings of Pusch et al.[1] and the model according to Ritchie[25] it is known that an increasing particle size and the associated greater distance between them correlates with an increase

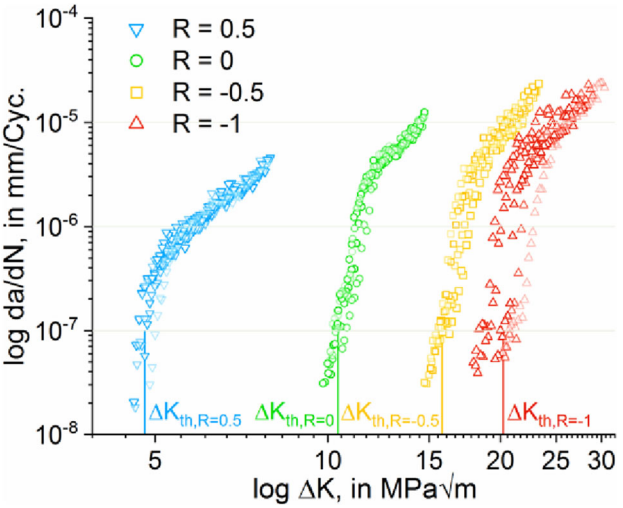

***Figure 9. Measured data for threshold determination on SENB-specimens at the sampling position main area (outside) as a function of* R.**

***Table 5. Mean Values of Threshold of All Sampling Positions as a Function of* R**

R	ΔK_{th}, in MPa$\sqrt{m}$			
	Main area (outside)	Shaft head	Main area (inside)	Shaft flange
0.5	4.8 ± 0.1	5.0 ± 0.2	5.1 ± 0.1	–
0	10.4 ± 0.2	10.2 ± 0.4	10.3 ± 0.6	–
− 0.5	15.8 ± 0.3	15.6 ± 0.4	16.6 ± 0.0	–
− 1	20.2 ± 1.2	18.9 ± 0.3	19.8 ± 0.6	18.5 ± 0.3

in threshold values for ferritic nodular cast iron. This is based on the increase of the free path length for dislocations in the matrix and accompanying increase in plastic deformation required for crack initiation. The experimental findings of the microstructural analysis and threshold determination on EN-GJS-600-3 suggest that this model is not applicable for the present pearlitic cast iron grade. Threshold values of all sampling positions were independent of the microstructural gradient. Apparently, the content of residual ferrite has an approximately equal influence on the threshold value behaviour during cyclic crack growth as a coarse-grained matrix. Therefore, it can be assumed that the threshold-increasing effect of increasing mean diameter and mean distance of the graphite nodules is offset by a simultaneously decreasing ferrite content. The scatter of the values and their standard deviations was attributed to the heterogeneity of the metallic matrix and the graphite particles of this nodular cast iron.

The relatively low threshold values at $R = -1$ in the shaft flange of the rotor shaft are shown in Figure 10. It must be assumed that the microstructure is the dominant parameter influencing the mechanical parameters. The influence of the microstructure gradient on the threshold values in dependence of the load ratio, on the other hand, is rather small. Therefore, it is concluded that the influence of the matrix dominates at low crack growth rates compared to the influence of the graphite nodules.

If the results of cyclic crack growth behaviour of the reference position shaft flange are used for future quality assurance purposes, it must be considered that the threshold behaviour of the damage-relevant main area is strongly underestimated.

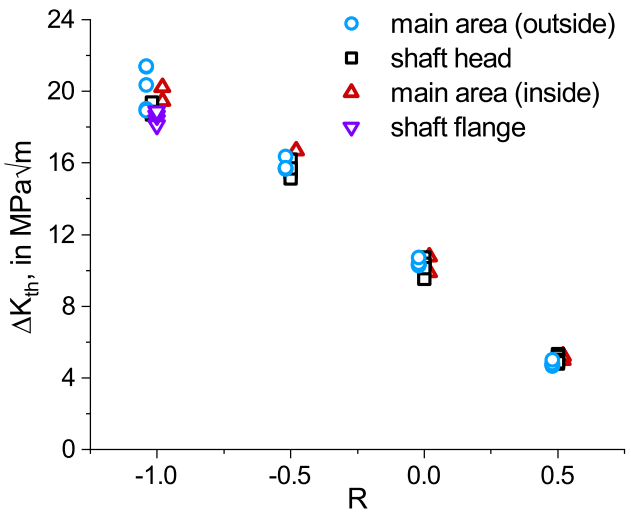

***Figure 10. Threshold values on SENB specimens of all sampling positions as a function of load ratio* R.**

The linear section of the cyclic crack growth curve describes stable crack propagation and can be expressed by the Paris Eqn. 1

$$\frac{da}{dN} = C \cdot \Delta K^m. \qquad \text{Eqn. 1}$$

The parameters m and C of the Paris area were determined at R = const. under load increase from a start value of cyclic stress intensity ΔK. This was accomplished using a constant force amplitude. Stable crack propagation can be described by linear regression of the logarithmized $da/dN - \Delta K$-values of all samples tested under a certain load ratio. For the present studies, the evaluation to determine the parameters m and C is not adequately described in the ASTM E647-15 and the regression was performed in a subjectively defined data range, in which the measured values exhibit the greatest possible linearity. Figure 11 shows how upper and lower limit of the range of the crack growth rate da/dN were set individually for each load ratio. The upper limit was defined at $da/dN_{max} = 10^{-4}$ mm/Cycle.

Figure 12 presents the well-known opposite tendency of the Paris parameters m and C. With an increasing value for m, a decreasing value for C was determined and vice versa. It is striking that the values from the highly loaded main area (outside) and the shaft head show a similar tendency, whereas the Paris parameters on samples from the inner layer are extremely pronounced and frame the values of the other sample layers. The purely pearlitic matrix of this sample layer with coarse structure and heterogeneous formation of the graphite nodules thus seem to lead to particularly high values for m and low values for C. With a less ductile and pearlitic matrix, faster crack growth is thus to be expected for a given load. The middle and outer sample layers, on the other hand, have a larger proportion of residual ferrite surrounding the graphite nodules.

These results contradict previous findings that the crack propagation behaviour of ferritic cast iron materials is largely independent of the size of the graphite nodules[1] and therefore independent of the sample position in cross section between a permanent mould and a sand core.[24] With the present results for a pearlitic nodular cast iron, it can also be confirmed that with local heterogeneities due to graphite degenerations, the crack growth rate increased.[9]

Furthermore, the correlation of decreasing values of m and decreasing threshold values cannot be exclusively confirmed here. As shown in Figure 12, m is smallest for all sample positions at $R = -1$. Towards larger load ratios, the curves for m each pass through a maximum. It can be concluded that there is a severe mean stress effect on stable crack propagation. Furthermore, crack propagation behaviour of pearlitic EN-GJS-600-3 in the Paris section

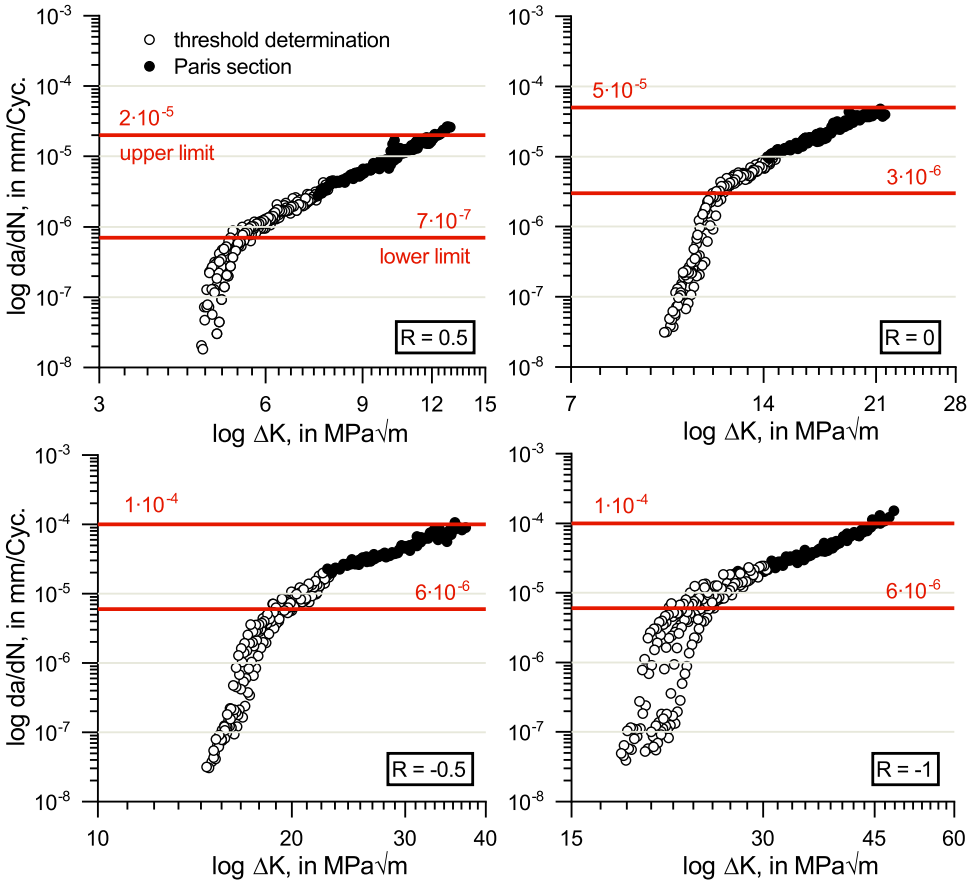

Figure 11. Upper and lower limit for linear regression as a function of* R*, test results of SENB-samples of the main area (outside).

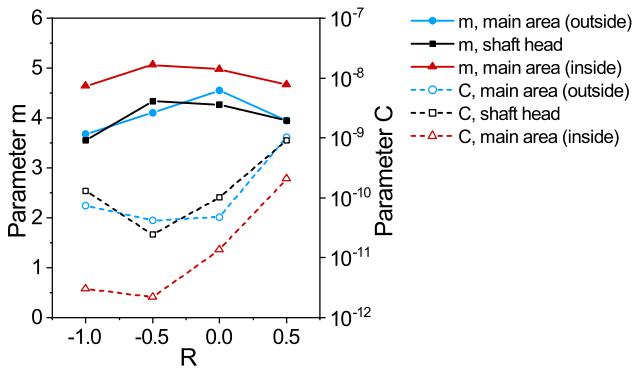

***Figure 12. Paris parameters* m *and* C *on SENB-specimens of the sampling positions main area and shaft head as a function of* R.**

differs clearly in a critical size and shape of graphite nodules and structure of the matrix.

Based on the findings of the present work, it is expected that threshold values at − 40 °C would be lower and crack growth rate in the section of stable crack growth would be greater than at room temperature due to embrittlement of the matrix and a decrease in plastic deformation.

Conclusion

The present work is intended to extend the knowledge of basic structure-property relationships on nodular cast iron components. While a broad basis has been developed in the past for traditional ductile cast iron materials for hollow rotor shafts, knowledge of higher-strength nodular cast iron in thick cross sections is still largely unexplored. The effect of a microstructure gradient on mechanical and fracture toughness properties is investigated on the present thick-walled EN-GJS-600-3 component using chill casting technology.

1. Metallographic analyses on specimens of all sample positions showed a clear dependence of the microstructure parameters on solidification conditions over the cross section of the thick-walled casting component. From the outer to the inner radius, the microstructure coarsened and became more heterogeneous. Residual ferrite in the pearlitic matrix decreased and was found predominantly in the shape of Bull's-eye ferrite.
2. It became clear that the fraction of ferritic phase, in addition to the graphite formation, has influenced mechanical properties and crack propagation resistance in fracture toughness evaluation in

various ways. The tensile characteristics of specimens of all sample positions generally exceed the characteristics required by the underlying normative standard DIN EN 1563 for the relevant nodular cast iron grade.

3. In dependence of the microstructure and thus of the sampling position in cross section, specimens showed a wide range of damage and failure behaviour and the evaluation of quasi-static fracture toughness had to be performed both in terms of elastic and elastic-plastic methods. A fine-grained and homogeneous microstructure resulted in increased fracture toughness at a low temperature of − 40 °C. While a high proportion of Bull's-eye ferrite seemed to influence the deformation capacity in front of the crack tip, unstable crack propagation could not be completely stopped.
4. The results of cyclic crack propagation tests, on the other hand, showed that threshold values were relatively little dependent on microstructure and the crack initiation process is only slightly influenced by the characteristics of the metallic matrix and graphite nodules. Degenerated graphite particles and the associated notch effect as well as a varying ductility of the matrix in this heterogeneous material lead to high scatter in the characteristic values for the cyclic threshold value behaviour.
5. Whereas in previous work on ferritic nodular cast iron it was found that stable crack growth in the Paris section was largely independent of microstructural parameters, the present investigation of different microstructural characteristics of EN-GJS-600-3 showed that a coarse structure and heterogeneous graphite formation seem to cause particularly high values for m and low values for C. In addition, crack propagation resistance depends on ferrite content in the pearlitic matrix and on the effect of mean stress during cyclic loading, too.
6. If the results of cyclic crack growth behaviour of the reference position shaft flange are used for future quality assurance purposes, it must be considered that especially the threshold behaviour of the damage-relevant main area is strongly underestimated.

Acknowledgements

The joint project "GussWelle" is carried out in collaboration with Fraunhofer LBF and IWES as well as the industry partners Nordex Energy SE & Co. KG and Walzengiesserei Coswig GmbH. The authors are grateful to the Federal Ministry of Economic Affairs and Energy for funding the joint project (0324329B) at the Institute of Materials Engineering (IWT) at the Technische Universität Bergakademie Freiberg.

Funding

Open Access funding enabled and organized by Projekt DEAL.

REFERENCES

1. G. Pusch, B. Komber, O. Liesenberg, Bruchmechanische Kennwerte für ferritische duktile Gusseisenwerkstoffe bei zyklischer Beanspruchung. konstruieren+gießen **21**(2), 54–59 (1996)
2. G. Pusch, S. Henkel, H. Biermann, P. Hübner, A. Ludwig, P. Trubitz, T. Mottitschka, L. Krüger, Determination of fracture mechanics parameters for cast iron materials under static, dynamic and cyclic loading, in *Recent Trends in Fracture and Damage Mechanics*. ed. by G. Hütter, L. Zybell (Springer, Cham, 2016), pp. 159–196. https://doi.org/10.1007/978-3-319-21467-2_7
3. T. Mottitschka, G. Pusch, H. Biermann, L. Zybell, M. Kuna, Influence of graphite spherical size on fatigue behaviour and fracture toughness of ductile cast iron EN-GJS-400-18LT. Int. J. Mater. Res. **103**(1), 87–96 (2012). https://doi.org/10.3139/146.110636
4. M. Riebisch, C. Seiler, B. Pustal, A. Bührig-Polaczek, Microstructure of as-cast high-silicon ductile iron produced via permanent mold casting. Inter. Metalcast. **13**, 112–120 (2019). https://doi.org/10.1007/s40962-018-0232-5
5. FKM-Guideline, Bruchmechanischer Festigkeitsnachweis für Maschinenbauteile—Fracture mechanical strength verification for machine components (2009)
6. F. Pollicino, Bruchmechanische Fragestellungen bei der Lebensdauerberechnung von Windenergieanlagen, in *Conference Arbeitskreis Bruchvorgänge, Deutscher Verband für Materialforschung und -prüfung e.V.* (Dresden, 2007), pp. 57–69
7. T. Borsato, P. Ferro, F. Berto, C. Carollo, Mechanical and fatigue properties of pearlitic ductile iron castings characterized by long solidification times. Eng. Fail. Anal. **79**, 902–912 (2017)

8. P. Canzar, Z. Tonkovic, J. Kodvanj, Microstructure influence on fatigue behaviour of nodular cast iron. Mater. Sci. Eng. A Struct. **556**, 88–99 (2012)
9. W. Baer, Chunky graphite in ferritic spheroidal graphite cast iron: formation, prevention, characterization, impact on properties: an overview. Inter. Metalcast. **14**, 454–488 (2020). https://doi.org/10.1007/s40962-019-00363-8
10. DIN 50125, Testing of metallic materials—tensile test pieces (2016)
11. ISO 12135, Metallic materials—unified method of test for the determination of quasistatic fracture toughness (2016)
12. ISO 12108, Metallic materials—fatigue testing—fatigue crack growth method (2018)
13. EN 1563, Founding—spheroidal graphite cast irons (2018)
14. M. Rüssel, L. Krüger, S. Martin, W. Kreuzer, Microstructural and fracture toughness characterisation of a high-strength FeCrMoVC alloy manufactured by rapid solidification. Eng. Fract. Mech. **99**, 278–294 (2013)
15. Y. Murakami, *Stress Intensity Factors Handbook* (Pergamon Books Ltd., New York, 1987)
16. ASTM E647-15e1, *Standard Test Method for Measurement of Fatigue Crack Growth Rates* (2016)
17. R.J. Bucci, Development of a proposed ASTM standard test method for near-threshold fatigue crack growth rate measurement. Symposia paper, ASTM International 5–28 (1981). https://doi.org/10.1520/STP33449S
18. VDMA 23902, Guideline for fracture mechanical strength assessment of planet carriers made of nodular cast iron EN-GJS-700-2 for wind turbine gear boxes (2014)
19. P. Trubitz, Werkstoffprüfung – nur ein (Hand)werkzeug des Ingenieurs? Gedanken zur Planung, Durchführung und Auswertung von Versuchen, in *Conference Werkstoffprüfung, Deutsche Gesellschaft für Materialkunde e.V.* (Neu-Ulm, 2016), pp. 49–58
20. P. Trubitz, K. Koch, S. Grützner, S. Hübner, L. Krüger, Contribution to the determination and numerical evaluation of cyclic crack propagation in GJS materials, in *Conference InCeight Casting C8*, (Darmstadt, 2021), pp. 47–60
21. ASTM E1820, *Standard Test Method for Measurement of Fracture Toughness* (2020)
22. S. Wolfensberger, P. Uggowitzer, M.O. Speidel, Die Bruchzähigkeit von Gusseisen - Teil II: Gusseisen mit Kugelgraphit. Gießereiforschung **39**, 2 (1987)
23. W. Baer, Advanced fracture mechanics testing of DCI—a key to valuable toughness data. Inter. Metalcast. **8**, 25–34 (2014). https://doi.org/10.1007/BF03355579
24. J.M. Motz, D. Berger, G. Cohrt, E.K. Godehardt, K. Hüttebräucker, G. Kuhn, H. Reuter, D. Schock, W. Shakeshaft, D. Wolters, Bruchmechanische Eigenschaften in großen Wanddicken von Gussstücken aus Gusseisen mit Kugelgraphit. Gießereiforschung **32**(3), 97–111 (1980)
25. R.O. Ritchie, Influence of microstructure on near-threshold fatigue crack propagation in ultra-high strength steel. Met. Sci. **11**(8/9), 368–381 (1977)